ORGANOMETALLICS

Article

pubs.acs.org/Organometallics

Experimental and Theoretical Study of the Effectiveness and Stability of Gold(I) Catalysts Used in the Synthesis of Cyclic Acetals

Jesús Cordón, José M. López-de-Luzuriaga,* and Miguel Monge

Departamento de Química, Centro de Investigación en Síntesis Química (CISQ), Complejo Científico-Tecnológico, Universidad de La Rioja, 26004 Logroño, La Rioja, Spain

Supporting Information

ABSTRACT: Different $[AuL]^+$ fragments (L = tertiary phosphines, ylides, or NHC carbene) have been tested under mild conditions as suitable catalysts for the transformation of terminal or internal alkynes into the corresponding cyclic acetals upon reaction with ethylene glycol. We have obtained a moderate to negligible activity when using tertiary phosphines or nonstabilized ylides as ligands. However, a very high catalytic activity is reached when the IPr N-heterocyclic carbene ligand is used. We have analyzed the key stages in this type of gold-catalyzed reaction, namely, (i) electronic activation (alkynophilicity); (ii) protodeauration; and (iii) decomposition of the gold catalyst. The first two stages have been analyzed through DFT computation of the minimum-energy reaction pathways employing different catalysts. An explanation of the catalysts' stability has been proposed through the analysis of *in situ* time-resolved nuclear magnetic resonance spectra of the catalysts.

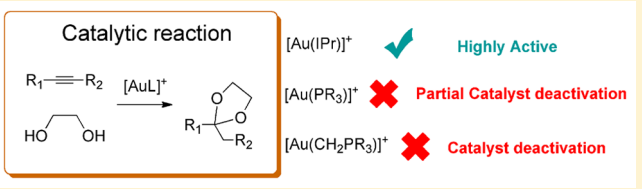

INTRODUCTION

The spectacular development of homogeneous gold catalysis in the last years has indirectly provided a good number of gold complexes that display an extraordinary ability as catalysts to promote an increasing variety of organic transformations of unsaturated precursors.[1−13] In the case of cationic complexes of the type $[AuL]^+$ (L = neutral ligand) recent reports have dealt with the importance of relativistic effects on the versatility and selectivity of these complexes as catalysts.[14−18] When gold is employed, the most important relativistic consequence from a catalytic point of view is the contraction of the 6s orbital, which is responsible for the exceptionally strong Au(I)−L bonds and the very high Lewis acidity of $[AuL]^+$ cationic species.[17,18] In the particular case of alkynes, these processes result from the unique ability of $[AuL]^+$ species to activate carbon−carbon triple bonds as soft, alkynophilic Lewis acids, thus promoting the attack of a nucleophile and a very high catalytic activity. This trend allows the formation of C−C, C−N, C−O, and C−S bonds by nucleophilic attack on the activated multiple bonds.[2]

However, in spite of the increasing number of new gold catalysts and organic transformations achieved, there are few systematic studies comparing the catalytic performance, effectiveness, and stability of different types of gold catalysts in a given organic transformation. In fact, in several cases the reaction conditions used in gold-catalyzed reactions exceed the needed catalyst loading, reaction time, or temperature for an efficient organic transformation. In a recent experimental report by Xu and co-workers[19] the authors categorized most of the gold-catalyzed reactions taking into account the influence exerted by the ancillary ligand (L, mostly tertiary phosphines) in the Au(I) center in three steps, namely, (i) electronic activation, (ii) protodeauration, and (iii) decomposition of the gold catalyst. In this study the authors established that the structure−activity relationship between the ancillary ligand and the kinetics of the minimum-energy pathway of the catalysis is not backed by experimental data in all cases. Similarly, the catalyst deactivation−ligand structure relationship is also difficult to elucidate.

Taking the above comments into account, we decided to study both experimentally and theoretically the gold-catalyzed synthesis of cyclic acetals from the corresponding alkynes and ethylene glycol as a benchmark reaction, using different types of $[AuL]^+$ catalysts (L = tertiary phosphines, ylides, or NHC carbene) (see Scheme 1). This reaction was previously studied experimentally by the use of $[AuCl(PPh_3)]/AgBF_4$, and,[20] as

Scheme 1. Ancillary Ligands (L) Used in $[AuL]^+$ Catalysts in This Work

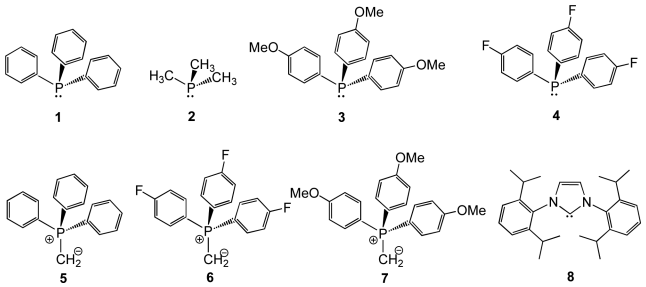

Received: December 17, 2015

DOI: 10.1021/acs.organomet.5b01015
Organometallics XXXX, XXX, XXX−XXX

far as we are aware, a systematic study of the alkynophilicity and stability of different gold(I) catalysts and the use of theoretical tools for a rational understanding of the mechanism of action of the gold catalysts have not been reported to date. Thus, from an experimental viewpoint we have checked the ability of different $[AuL]^+$ catalysts toward the transformation of several alkynes into cyclic acetals, but we have also focused on the stability of the catalyst during the whole catalytic process through time-resolved NMR experiments. From a theoretical point of view we have focused on the description of the complete minimum-energy reaction pathway for the transformation of phenylacetylene into the corresponding cyclic acetal, using different $[AuL]^+$ model catalysts and paying also special attention to the ethylene glycol assistance for a more correct description of the protodeauration step. We have finally compared the experimental and theoretical results in order to explain if any of the above-mentioned steps, i.e., electronic activation, protodeauration, and catalyst decompositions, play an important role in the catalyzed synthesis of cyclic acetals.

RESULTS AND DISCUSSION

Synthesis and Characterization of the Catalysts. Compounds $[AuClPPh_3]$[21] (**1**), $[AuClPMe_3]$[22] (**2**), $[AuClP(C_6H_4OMe)_3]$[23] (**3**), and $[AuCl(IPr)]$[24] (**8**) were synthesized according to the published procedures.

The complex $[AuClP(C_6H_4F)_3]$ (**4**) was prepared by reaction of (4-fluorophenyl)phosphine with [AuCl(tht)] in dichloromethane as reported previously by Laguna et al.[25] Briefly, the compounds $[AuCl(CH_2P(R)_3)]$ (R = (C_6H_5) (**5**), (C_6H_4F) (**6**), (C_6H_4OMe) (**7**)) were prepared using a two-step procedure. In the first step, reaction of the phosphonium salt, $[P(R)_3Me]ClO_4$, with butyllithium and $[Au(C_6F_5)(tht)]$ led to the formation of the corresponding $[Au(C_6F_5)(CH_2P(R)_3)]$ (R = C_6H_5, C_6H_4F, C_6H_4OMe) neutral precursors. The reaction of these compounds with excess of HCl in diethyl ether at −10 °C produced the precipitation of compounds **5**, **6**, and **7** as white solids.

The formation of the expected complexes was checked through ^1H, ^{19}F, and $^{31}P\{^1H\}$ NMR and IR spectroscopy. For instance, the ^{31}P NMR spectra of compounds **4**−**7** display a singlet at 30.87 ppm (**4**), 30.31 ppm (**5**), 29.14 ppm (**6**), and 27.94 ppm (**7**), respectively, corresponding to the P-containing ligands bonded to Au(I). In addition, in the ^1H NMR spectra of compounds **5**−**7** a doublet appears at 2.12 ppm (**5**), 2.09 ppm (**6**) and 2.02 ppm (**7**), due to the CH_2 protons of the ylide ligands.

Synthesis of Cyclic Acetals. Experimental Study. We tested the catalytic performance of catalysts of the type $[AuL]^+$, prepared *in situ* by reaction of the corresponding chlorogold(I) complexes **1**−**8** with 1 equiv of AgTfO (TfO = trifluoromethylsulfonate), in the reaction of different alkynes with ethylene glycol in toluene at 100 °C, during 4 h and under an argon atmosphere (see Scheme 2). The results of these experiments are shown in Table 1.

The results obtained for the catalytic conversions with the phosphinogold(I) compounds **1**−**4** under these high temperature catalytic conditions show that the conversion for all of them reaches at least 91% with a 2% mol catalyst loading, being complete when complexes **1**, **3**, and **4** (>99%) are employed. The result obtained in entry 1 is similar to the one reported by Santos et al. using the $[AuCl(PPh_3)]/AgBF_4$ couple instead of the $[AuCl(PPh_3)]$/AgTfO one.[20] On the other hand, the results of the catalysis with the ylidegold(I) compounds **5**−**7** show that complex **7** at 2% mol catalyst loading reaches >99% conversion, being higher than with complex **6** (88%) or compound **5** (54%). We also observe that in the case of the NHC−gold(I) derivative **8** a complete conversion (>99%) is obtained with these experimental conditions. Apart from the poorer, although non-negligible conversions obtained with ylidegold(I) catalysts **5** and **6**, it seems that under the reaction conditions employed a very good performance in the formation of 2-methyl-2-phenyl-1,3-dioxolane is achieved with these three types of cationic gold(I) catalysts.

As mentioned before, the nature of the ligand L in the cationic phosphinogold(I) catalysts was expected to exert an important influence on the catalytic activity of the addition of methanol to propyne, promoting electron-poor ligands, an increase in activity that was concomitant with the decrease of the catalyst stability.[26] Taking into account this and the fact that using the above-mentioned catalytic conditions no clear differences among the employed catalysts were detected, we repeated the experiments using milder catalytic conditions, i.e., toluene at 75 °C during 1 h and a similar catalyst loading (2%) (see Table 2).

The results given in Table 2 are more informative. First of all, it is worth mentioning that under mild conditions the only catalyst leading to quantitative formation of 2-methyl-2-phenyl-1,3-dioxolane was catalyst $[Au(IPr)]^+$ (**8**); instead, phosphine-based catalysts **1**−**4** lead to intermediate conversions, and ylide-based catalysts **5**−**7** give rise even to poorer conversions of phenylacetylene into the corresponding cyclic acetal. In addition, the electron-poor phosphine ligand $P(C_6H_4F)_3$ leads to a better conversion than the electron-rich one PMe_3, in agreement with the previously reported results.[26] However, this trend is not observed for the ylide case, for which the electron-poorer ylide ligand $CH_2P(C_6H_4F)_3$ leads to the worst conversion. These experimental results would point to an important role played by the catalyst stability under the studied conditions (*vide infra*).

Scheme 2. Synthesis of Cyclic Acetals and Alkynes Used in This Work

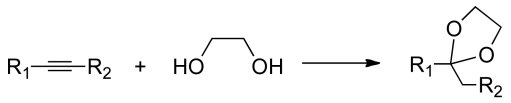

R_1 = Ph, C_4H_9, $C_{10}H_{21}$, ^{t}Bu; R_2 = H
R_1 = Ph; R_2 = Ph, CH_3

Table 1. Transformation of Phenylacetylene into 2-Methyl-2-phenyl-1,3-dioxolane at 100 °C during 4 h

entry	catalyst[a]	conversion (%)[b]
1	$[Au(PPh_3)]^+$	>99
2	$[Au(PMe_3)]^+$	91
3	$[Au\{P(C_6H_4OMe)_3\}]^+$	>99
4	$[Au\{P(C_6H_4F)_3\}]^+$	>99
5	$[Au(CH_2PPh_3)]^+$	54
6	$[Au\{CH_2P(C_6H_4F)_3\}]^+$	88
7	$[Au\{CH_2P(C_6H_4OMe)_3\}]^+$	>99
8	$[Au(IPr)]^+$	>99

[a]All the catalysts were prepared by addition of 1 equiv of AgTfO to the corresponding [AuClL] precursor, leading to a 2% catalyst loading. [b]Conversion to 2-methyl-2-phenyl-1,3-dioxolane determined by GC-MS.

DOI: 10.1021/acs.organomet.5b01015
Organometallics XXXX, XXX, XXX−XXX

Table 2. Transformation of Phenylacetylene into 2-Methyl-2-phenyl-1,3-dioxolane at 75 °C during 1 h

entry	catalyst[a]	conversion (%)[b]
1	$[Au(PPh_3)]^+$	48
2	$[Au(PMe_3)]^+$	19
3	$[AuP(C_6H_4OMe)_3]^+$	35
4	$[AuP(C_6H_4F)_3]^+$	46
5	$[Au(CH_2PPh_3)]^+$	12
6	$[Au(CH_2P(C_6H_4F)_3)]^+$	4
7	$[Au(CH_2P(C_6H_4OMe)_3)]^+$	6
8	$[Au(IPr)]^+$	>99

[a]All the catalysts were prepared by addition of 1 equiv of AgTfO to the corresponding [AuClL] precursor, leading to a 2% catalyst loading. [b]Conversion to 2-methyl-2-phenyl-1,3-dioxolane determined by GC-MS.

Because ylide−gold(I) compounds led to the worst catalytic performance toward the formation of 2-methyl-2-phenyl-1,3-dioxolane under mild reaction conditions, we focused on the experimental comparison between P-based catalyst $[Au(PPh_3)]^+$ and the NHC-containing one $[Au(IPr)]^+$. For this we checked the catalytic formation of other cyclic acetals using different terminal alkynes such as 1-dodecyne, 1-hexyne, and *tert*-butylacetylene or internal alkynes such as diphenylacetylene and 1-phenyl-1-propyne.

The results depicted in Table 3 also relay interesting information. Thus, when the substituent of the alkyne is an aliphatic chain, both catalysts are very effective under mild reaction conditions, leading to complete formation of the corresponding cyclic acetal. However, when the substituent is a bulky *tert*-butyl group (entries 9, 10) or a phenyl one (entries 1, 2), the NHC−gold(I) catalyst still leads to a quantitative formation of the cyclic acetal (>99%), whereas the $[Au(PPh_3)]^+$ catalyst gives rise to only a 48% (entry 1) or 56% (entry 9) conversion. In the case of internal alkynes also the $[Au(IPr)]^+$ catalyst performs better than $[Au(PPh_3)]^+$. When diphenylacetylene is used, only 1% and 11% conversion is achieved with $[Au(PPh_3)]^+$ and $[Au(IPr)]^+$, respectively, whereas when 1-phenyl-1-propyne is employed, the conversions rise to 7% and 89%, respectively, probably due to less steric hindrance in the latter cases. Again, the catalytic performance of the $[Au(IPr)]^+$ species is better than the $[Au(PPh_3)]^+$ one, regardless of the alkyne tested.

Table 3. Transformation of Different Alkynes into Cyclic Acetals at 75 °C during 1 h

entry	alkyne	catalyst[a]	Conv. (%)[b]
1	Ph—≡—H	$[Au(PPh_3)]^+$	48
2	Ph—≡—H	$[Au(IPr)]^+$	>99
3	Ph—≡—Ph	$[Au(PPh_3)]^+$	1
4	Ph—≡—Ph	$[Au(IPr)]^+$	11
5	$C_{10}H_{21}$—≡—H	$[Au(PPh_3)]^+$	>99
6	$C_{10}H_{21}$—≡—H	$[Au(IPr)]^+$	>99
7	C_4H_9—≡—H	$[Au(PPh_3)]^+$	>99
8	C_4H_9—≡—H	$[Au(IPr)]^+$	>99
9	^{t}Bu—≡—H	$[Au(PPh_3)]^+$	56[c]
10	^{t}Bu—≡—H	$[Au(IPr)]^+$	99[c]
11	Ph—≡—CH_3	$[Au(PPh_3)]^+$	7[d]
12	Ph—≡—CH_3	$[Au(IPr)]^+$	89[e]

[a]All the catalysts were prepared by addition of 1 equiv of AgTfO to the corresponding [AuClL] precursor, leading to a 2% catalyst loading. [b]Conversion determined by GC-MS. [c]Markovnikov regioselectivity preference for $[AuCl(PPh_3)]$/AgTfO (96%) and $[AuCl(IPr)]$/AgTfO (95%) catalysts. [d]50% nucleophilic addition to each triple-bond position. [e]82% nucleophilic addition to the C atom bonded to the methyl group.

We also studied this catalytic process under mild conditions (75 °C during 1 h) at different reaction times. Again, the performance of the $[Au(IPr)]^+$ catalyst is much better than $[Au(PPh_3)]^+$, leading to a complete conversion into the corresponding cyclic acetal after 15 min of reaction, whereas the triphenylphosphino gold(I) catalyst achieves only a maximum of 42% conversion after 45 min of reaction when phenylacetylene is used, and it needs 30 min for the quantitative transformation of 1-dodecyne (see Table 4).

Table 4. Transformation of Different Alkynes into Cyclic Acetals at 75 °C during 1 h, at Different Reaction Times

entry	alkyne	catalyst[a]	Time (min)	Conv (%)[b]
1	Ph—≡—H	$[Au(PPh_3)]^+$	15	16
2			30	24
3			45	42
4	Ph—≡—H	$[Au(IPr)]^+$	15	99
5			30	>99
6	$C_{10}H_{21}$—≡—H	$[Au(PPh_3)]^+$	15	95
7			30	>99
8	$C_{10}H_{21}$—≡—H	$[Au(IPr)]^+$	15	>99

[a]All the catalysts were prepared by addition of 1 equiv of AgTfO to the corresponding [AuClL] precursor. [b]Conversion determined by GC-MS.

In view of these experimental results, we envisioned that one of the three previously mentioned stages (stage 1: alkyne activation; stage 2: protodeauration; or stage 3: catalyst decomposition) should be responsible for the clear differences found for the different types of Au(I) catalysts tested experimentally under mild conditions. It is important to note that many of the Au(I)-catalyzed hydration processes of alkynes described in the literature could be revisited in terms of the efficient use of catalytic species and chemical sustainability. In order to fully address this issue, we have carried out an in-depth theoretical (DFT) and experimental (NMR spectroscopy) study of the different steps in the transformation of phenylacetylene into 2-methyl-2-phenyl-1,3-dioxolane. The theoretical part is devoted to the study of the alkyne activation and protodeauration steps (1 and 2), whereas the spectroscopic part of the study is focused on the possible catalyst decomposition (3).

Theoretical Study: Alkyne Activation and Protodeauration Steps. Taking into account the different results obtained in the catalyzed synthesis of cyclic acetals using different cationic Au(I) catalysts and reaction conditions, we

DOI: 10.1021/acs.organomet.5b01015
Organometallics XXXX, XXX, XXX−XXX

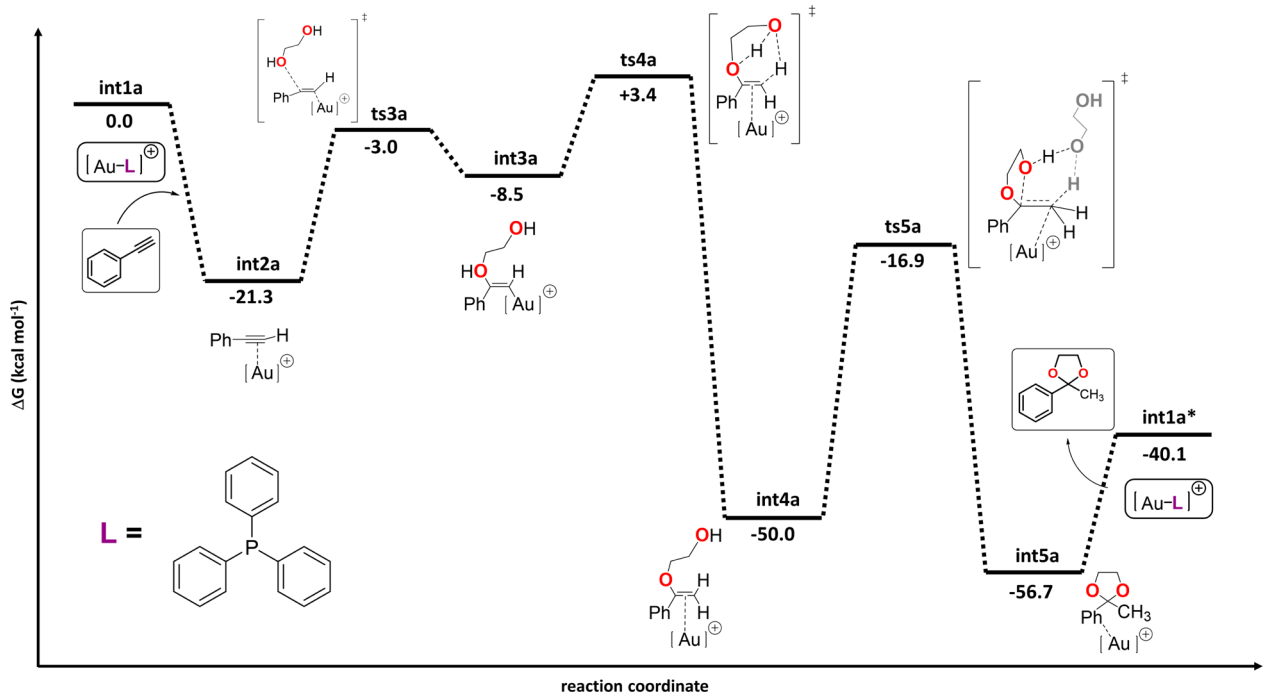

Figure 1. Complete minimum-energy reaction pathway calculated for the proposed mechanism of formation of 2-methyl-2-phenyl-1,3-dioxolane, catalyzed by model $[Au(PPh_3)]^+$ (**C**), at the DFT/M06-2X level. Relative Gibbs free energies (ΔG) are given in kcal mol^{-1}.

envisaged the use of computational tools in order to propose a minimum-energy reaction pathway and a plausible catalytic cycle. Apart from the complete characterization of the minimum-energy reaction pathway, the aim of these calculations is to compare the alkynophilicity exerted by the different $[Au(L)]^+$ (int2) catalysts leading to the formation of the corresponding *trans*-alkenyl gold complex (int3) intermediate and the energetic barriers of the protodeauration (int4–int5) steps. As recently shown Xu and co-workers, these are two of the three major stages of the gold(I)-catalyzed activation of alkynes together with the deactivation of the catalyst.[19]

Figures 1 and 2 depict the minimum-energy pathway calculated at the DFT/M06-2X level for a proposed mechanism of formation of 2-methyl-2-phenyl-1,3-dioxolane, using model systems $[Au(PPh_3)]^+$ (**C**), $[Au(CH_2P(C_6H_4OMe))]^+$ (**F**), and $[Au(IPr)]^+$ (**G**) as catalysts. We have also evaluated this minimum-energy pathway using other model systems, changing the L neutral ligand, but we will compare in the next paragraphs among the minimum-energy pathways for these three catalysts as a representative example. Thus, for example, we have computed the results using the PH_3 ligand, which is the simplest model system for a Au(I)–tertiary phosphine catalyst, giving, with much less computational cost, a prompt picture of the reaction mechanism (see Figure S1). Table 5 displays the energy of the minimum-energy pathway critical points using all the studied model systems: $[Au(PH_3)]^+$ (**A**), $[Au(PMe_3)]^+$ (**B**), $[Au(PPh_3)]^+$ (**C**), $[Au(CH_2PPh_3)]^+$ (**D**), $[Au(CH_2P(C_6H_4F)_3)]^+$ (**E**), $[Au(CH_2P(C_6H_4OMe)_3)]^+$ (**F**), and $[Au(IPr)]^+$ (**G**).

In this pathway, using catalysts $[Au(PPh_3)]^+$ (**C**), $[Au(CH_2P(C_6H_4OMe))]^+$ (**F**), and $[Au(IPr)]^+$ (**G**), the catalytic cycle starts with an electronic activation of the alkyne by the approach of phenylacetylene to the $[Au(L)]^+$ fragment, which leads to a stabilization in the 16.1–22.0 kcal mol^{-1} range depending on the Au(I) catalyst, the largest stabilization energies being the ones corresponding to Au(I)–PPh_3 and

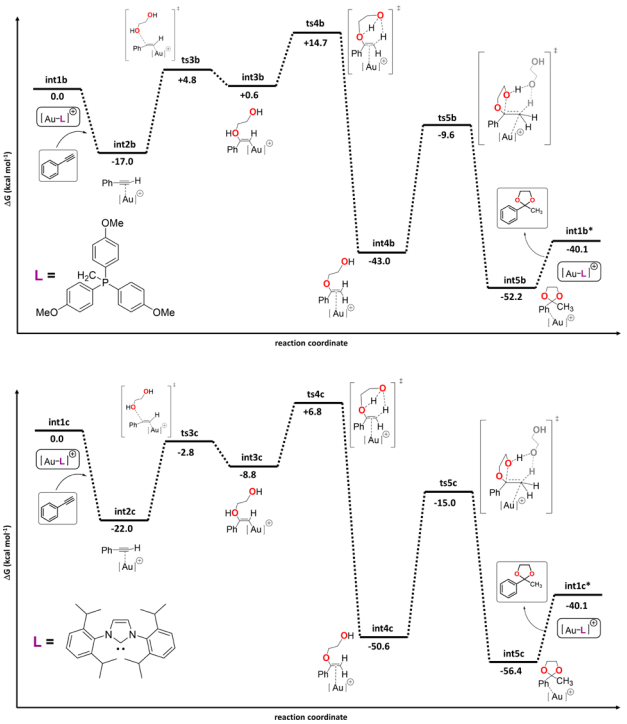

Figure 2. Complete minimum-energy reaction pathway calculated for the proposed mechanism of formation of 2-methyl-2-phenyl-1,3-dioxolane, catalyzed by model $[Au(CH_2P(C_6H_4OMe))]^+$ (**F**) (top) or by model $[Au(IPr)]^+$ (**G**) (bottom), at the DFT/M06-2X level. Relative Gibbs free energies (ΔG) are given in kcal mol^{-1}.

Au(I)–NHC catalysts (see Table 5). We have evaluated the alkynophilicity displayed by models $[Au(PPh_3)]^+$ (**C**), $[Au(CH_2P(C_6H_4OMe))]^+$ (**F**), and $[Au(IPr)]^+$ (**G**) by the estimation of the counterpoise correction to the basis set superposition error (BSSE) at different points of the reaction

DOI: 10.1021/acs.organomet.5b01015
Organometallics XXXX, XXX, XXX–XXX

Table 5. Relative Gibbs Free Energies (ΔG, in kcal mol^{-1}) Calculated for the Minimum-Energy Pathway Critical Points (Intermediates and Transition States) for Model Systems A−G

	int1	int2	ts3	int3	ts4	int4	ts5	int5	int1*
$[Au(PH_3)]^+$ **A**	0.0	−21.9	−6.6	−13.9	+1.1	−52.1	−19.6	−57.0	−40.1
$[Au(PMe_3)]^+$ **B**	0.0	−17.3	+0.5	−5.5	+9.0	−47.1	−13.3	−53.3	−40.1
$[Au(PPh_3)]^+$ **C**	0.0	−21.3	−3.0	−8.5	+3.4	−50.0	−16.9	−56.7	−40.1
$[Au(CH_2PPh_3)]^+$ **D**	0.0	−16.1	+4.1	−0.8	+13.0	−43.9	−13.5	−53.2	−40.1
$[Au(CH_2P(C_6H_4F)_3)]^+$ **E**	0.0	−17.8	+1.5	−2.8	+10.0	−44.8	−13.0	−54.1	−40.1
$[Au(CH_2P(C_6H_4OMe)_3)]^+$ **F**	0.0	−17.0	+4.8	+0.6	+14.7	−43.0	−9.6	−52.2	−40.1
$[Au(IPr)]^+$ **G**	0.0	−22.0	−2.8	−8.8	+6.8	−50.6	−15.0	−56.4	−40.1

coordinate (see Computational Details). Thus, if we calculate the alkynophilicity strength for the activation of the phenylacetylene (int2), we observe that the $[Au(IPr)]^+$ (**G**) catalyst displays the strongest interaction (ca. 41.0 kcal mol^{-1}), the $[Au(CH_2P(C_6H_4OMe))]^+$ (**F**) catalyst is intermediate (ca. 37.0 kcal mol^{-1}), and $[Au(PPh_3)]^+$ (**C**) displays the lowest alkynophilicity strength (ca. 36.5 kcal mol^{-1}). However, the difference in energy for the alkynophilicity among the three catalysts is not significant. We have also accounted for the strength of the Au−π interactions by measuring the Au−C distances and the loss of linearity of the phenylacetylene moiety (see Table S1).

In the next step one ethylene glycol molecule reacts with the internal position of the triple bond of the predistorted alkyne (ts3, Markovnikov regioselectivity). The experimentally obtained products correspond in all cases to this regioselectivity. The obtained intermediate int3 is more stable for catalysts $[Au(IPr)]^+$ (**G**) (−8.8 kcal mol^{-1}) and $[Au(PPh_3)]^+$ (**C**) (−8.5 kcal mol^{-1}) than for $[Au(CH_2P(C_6H_4OMe))]^+$ (**F**) (+0.6 kcal mol^{-1}). The next process consists of a proton transfer from the oxygen already attached to the alkene to the terminal carbon of the same, through the transition state ts4. This process is assisted by the participation of the other OH group of the ethylene glycol molecule (Figures 1 and 2). This transition state is the highest point on the whole potential energy surface, with activation energy of +3.4 (**C**), +14.7 (**F**), and +6.8 kcal mol^{-1} (**G**). However, this step benefits the thermodynamics of the reaction, yielding an exergonic process (ΔG = −50.0 (**C**), −43.0 (**F**), and −50.6 kcal mol^{-1} (**G**)) with respect to the reactants, in which a disubstituted alkene intermediate (int4) is formed. We have also evaluated the strength displayed by the Au−π bonds in the transition state ts4 when using models $[Au(PPh_3)]^+$ (**C**), $[Au(CH_2P(C_6H_4OMe))]^+$ (**F**), and $[Au(IPr)]^+$ (**G**) by the estimation of the counterpoise correction to the BSSE (see Computational Details). We observe that the $[Au(PPh_3)]^+$ (**C**) catalyst displays the strongest interaction (ca. 102 kcal mol^{-1}), the $[Au(IPr)]^+$ (**G**) catalyst is intermediate (ca. 101 kcal mol^{-1}), and $[Au(CH_2P(C_6H_4OMe))]^+$ (**F**) displays the lowest Au−π strength (ca. 92 kcal mol^{-1}). Nevertheless, these values also represent fairly similar interaction strengths to the case of int2.

The next stage corresponds to the attack of the second OH group to form the corresponding cyclic acetal through a transition state that would include two steps in one, nucleophilic attack and proton transfer (ts5), leading to protodeauration. This process would be assisted by other ethylene glycol molecule (see Figures 1 and 2). In addition, at the end of this step (int5), the catalyst still maintains an interaction with the phenyl group of the final product. In this part of the minimum-energy profile the energies displayed for the transition state **ts5** are very similar regardless of the catalyst, i.e., −16.9 (**C**), −9.6 (**F**), and −15.0 kcal mol^{-1} (**G**). However, taking into account the stabilization energies computed for the corresponding intermediate int4, the largest activation energy barrier for this step corresponds to catalyst $[Au(IPr)]^+$ (**G**) (35.6 kcal mol^{-1}), being lower for catalysts $[Au(CH_2P(C_6H_4OMe))]^+$ (**F**) (33.4 kcal mol^{-1}) and $[Au(PPh_3)]^+$ (**C**) (33.1 kcal mol^{-1}). Taking into account these results, this would be the largest energy span computed for the three energy profiles and would be in agreement with a faster reaction when using catalysts $[Au(CH_2P(C_6H_4OMe))]^+$ (**F**) and $[Au(PPh_3)]^+$ (**C**). However, the experimental results are not in agreement with this trend. At this point it is worth mentioning that when the minimum-energy reaction pathway is computed using $[Au(IPr)]^+$ (**G**) and $[Au(PPh_3)]^+$ (**C**) as catalysts, the reaction intermediates are, in general, more stable than the ones obtained when $[Au(CH_2P(C_6H_4OMe))]^+$ (**F**) is used (see Table 5). In this regard, Table 6 and Figure 3 depict the comparison between the percent conversion and the stabilization energy of int4 with the different catalysts **B**, **C**, **D**, **F**, and **G**. As observed, there is a clear correlation between the stabilization of the intermediate (int4) and the percent of

Table 6. Comparison between the Percent Conversion and the Stabilization of int4 (ΔG in kcal mol^{-1}) for Catalysts B, C, D, F, and G

catalyst	conversion (%)	int4 ΔG
B	48	−47.1
C	19	−50.0
D	12	−43.9
F	6	−43.0
G	>99	−50.6

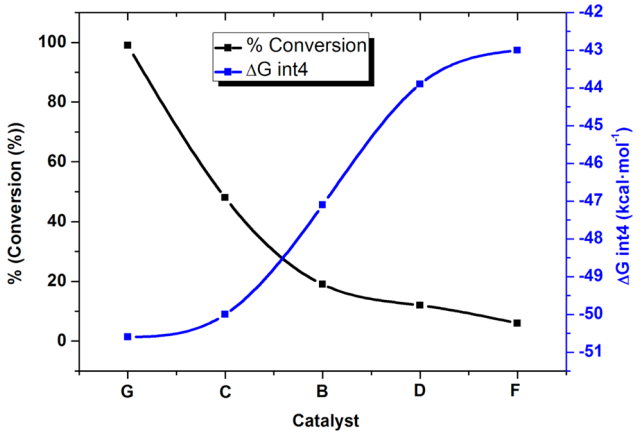

Figure 3. Comparison between the conversion and the int4 energy.

DOI: 10.1021/acs.organomet.5b01015
Organometallics XXXX, XXX, XXX−XXX

experimentally measured conversion. The most striking result is the extremely good conversion for catalyst $[Au(IPr)]^+$ (**G**), the int4 formed with this catalyst being only slightly more stable than the one obtained with $[Au(PPh_3)]^+$ (**C**) as catalyst. This observation and the experimental results prompted us to study the stability of the catalysts through nuclear magnetic resonance spectroscopy (*vide infra*). In addition, although we have computed the second nucleophilic attack and the protodeauration step assisted by an additional ethylene glycol molecule, recent studies on the role played by the counterion in the NHC−gold(I)-catalyzed alkoxylation of alkynes point to an important role played by the anion as a proton shuttle in the protodeauration step.[27] Also, a recent study by Díaz-Requejo, Pérez, and co-workers[28] evidenced an inner-sphere mechanism for NHC−Au(I)-catalyzed carbene-transfer reactions from ethyl diazoacetato, in which the coordination of the solvent/substrate to the Au(I) catalyst is proposed.[29]

In the last step of the mechanism, the catalyst breaks the interaction with the final product and is ready to continue a new cycle. Overall, the synthesis of cyclic acetals catalyzed by $[AuL]^+$ (L = tertiary phosphine, ylide, or N-heterocyclic carbene) is exergonic by −40 kcal mol^{-1}.

In view of the results obtained both experimentally and theoretically, we propose the catalytic cycle depicted in Scheme 3 for the synthesis of cyclic acetals catalyzed by gold(I) compounds of type $[Au\text{-}L]^+$.

Scheme 3. Proposed Catalytic Cycle after Experimental and Theoretical Studies

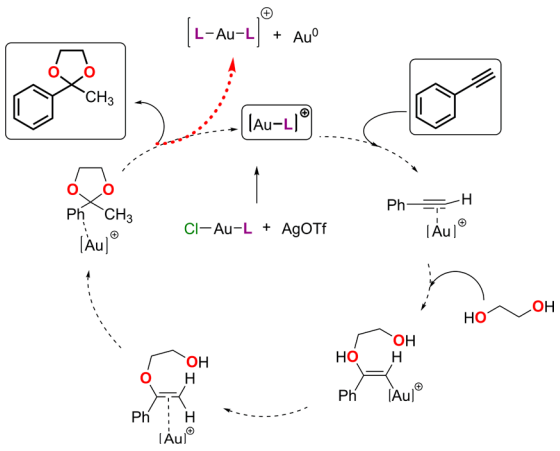

Nuclear Magnetic Resonance Study: Catalyst Stability. As it has been described above, the minimum-energy pathways computed at the DFT level for a proposed mechanism of formation of 2-methyl-2-phenyl-1,3-dioxolane using different catalysts point to a similar alkynophilicity for the catalysts regardless of the ligand bonded to Au(I) and a larger energy span for the experimentally better catalyst $[Au(IPr)]^+$. The fact that the experimental conversion can be correlated with the stability of the intermediate int4 made us wonder about the large differences found experimentally for the precentage of conversion, under mild reaction conditions, between the $[Au(IPr)]^+$ (**G**) catalyst and the rest of the Au(I) catalysts tested. In this regard, if the alkynophilicity or the protodeauration steps were not behind this behavior, we needed an alternative explanation for the, in principle, very good activity computed for the three types of catalysts. In order to explain the different behavior between catalysts $[Au(PPh_3)]^+$ (**B**), $[Au(CH_2P(C_6H_4OMe)_3)]^+$ (**F**), and $[Au(IPr)]^+$ (**G**), we focused on their stabilities in solution during the catalysis, which is the third key factor together with the alkynophilicity and protodeauration steps that clearly influence the kinetics of gold-catalyzed reactions. In order to gain insight into the stability of the catalysts, we carried out a time-resolved NMR study in order to follow the evolution of the catalyst before, during, and at the end of the catalytic process (see Figures 4−6).

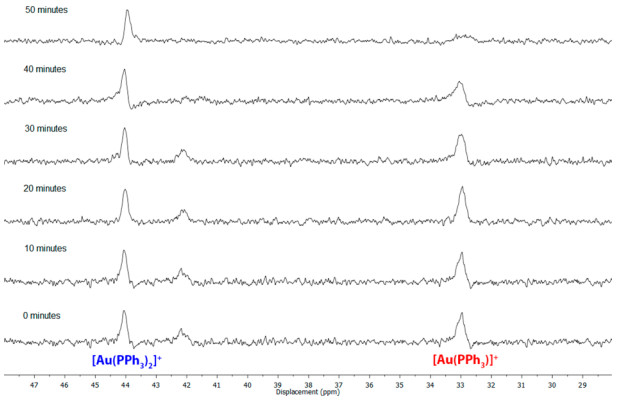

Figure 4. Time-resolved $^{31}P\{^1H\}$ NMR of catalyst $[Au(PPh_3)]^+$ (**C**) during the synthesis of 2-methyl-2-phenyl-1,3-dioxolane under mild conditions.

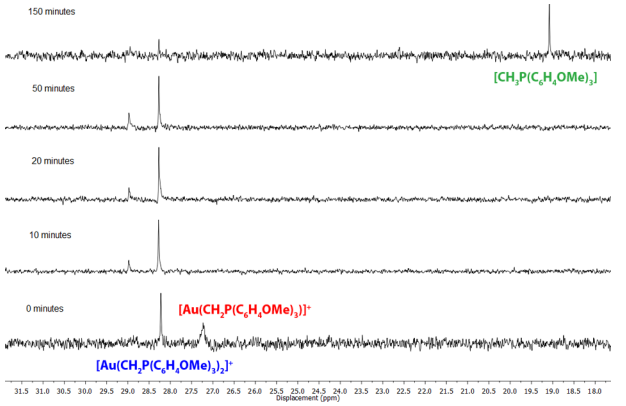

Figure 5. Time-resolved $^{31}P\{^1H\}$ NMR of catalyst $[Au(CH_2P(C_6H_4OMe)_3)]^+$ (**F**) during the synthesis of 2-methyl-2-phenyl-1,3-dioxolane under mild conditions.

In the case of catalyst $[Au(PPh_3)]^+$ (**C**) we observe how all the catalyst (signal at 33.0 ppm) is almost completely converted into nonactive $[Au(PPh_3)_2]^+$ (signal at 44.1 ppm)[30] after 50 min (see Scheme 4 and the Supporting Information). This result indicates that although the $[Au(PPh_3)]^+$ fragment would be a good catalyst for the synthesis of cyclic acetals under mild conditions, as it has been shown through DFT calculations, it is deactivated through the formation of the bis(phosphine)gold(I) inactive cation and metallic gold, even at short reaction times, as also observed experimentally.(Figure S2).

When $[Au(CH_2P(C_6H_4OMe)_3)]^+$ (**F**) is used as catalyst, we also observe a very fast evolution (10 min) of this cationic fragment (signal at 27.2 ppm) into the corresponding inactive $[Au(CH_2P(C_6H_4OMe)_3)_2]^+$ (signal at 28.3 ppm) and metallic gold. Longer reaction times (150 min) even give rise to the protonation of the phosphonium salt (signal at 19.1 ppm) and

DOI: 10.1021/acs.organomet.5b01015
Organometallics XXXX, XXX, XXX−XXX

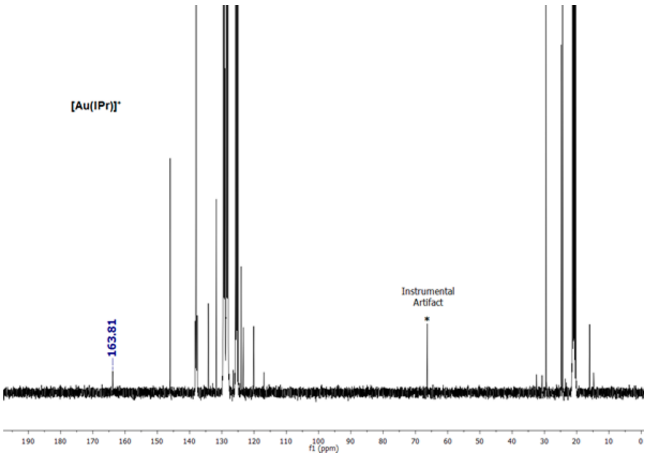

Figure 6. $^{13}C\{^1H\}$ NMR of catalyst $[Au(IPr)]^+$ (**G**) after 24 h in solution.

further inactive metallic gold formation (see Scheme 4). In this case, the very fast catalyst deactivation is in agreement with the very poor catalytic activity of gold(I)-ylide catalysts under the present reaction conditions.

As we have mentioned above, when we use catalyst $[Au(IPr)]^+$ (**G**), a quantitative conversion of phenylacetylene is achieved in only 15 min. This observation is in agreement with a higher stability of catalyst $[Au(IPr)]^+$ (**G**) (see Scheme 4) during the catalytic transformation and could explain its enhanced catalytic activity under mild conditions if compared to the rest of the catalysts. Figures 6 and S3 (with signal assignment) depict the $^{13}C\{^1H\}$ NMR spectrum of $[Au(IPr)]^+$ (**G**) formed *in situ* and kept in solution for more than 24 h. We observe that the pattern corresponds to the unaltered catalyst.[31]

CONCLUSIONS

In summary, we can conclude that among the three key steps governing the kinetics of gold-catalyzed reactions, namely, (i) electronic activation (alkynophilicity), (ii) protodeauration, and (iii) decomposition of the gold catalyst, the latter plays a very important role when mild reaction conditions are used in the synthesis of cyclic acetals. Thus, if the catalysis proceeds at higher temperatures, all Au(I) cationic species are good or very good catalysts. However, when milder catalytic conditions are employed, the larger reaction times needed for a quantitative conversion of the alkynes make the catalysis deactivation pathway a key parameter for the explanation of the lower conversions found for phosphine- and ylide-based Au(I) catalysts.

EXPERIMENTAL SECTION

General Procedures. The compounds $[AuClPPh_3]$[21] (**1**), $[AuClPMe_3]$[22] (**2**), $[AuClP(C_6H_4OMe)_3]$[23] (**3**), $[AuCl(IPr)]$[24] (**8**), $[PPh_3Me]ClO_4$,[32] and $[Au(C_6F_5)(CH_2PPh_3)]$[25] were synthesized according to the published procedure. Silver trifluoromethanesulfonate was purchased from Aldrich, while methyl iodide, tris(4-fluorophenyl)-phosphine, and tris(4-methoxyphenyl)phosphine were acquired from Alfa. Infrared spectra were recorded in the 4000−220 cm^{-1} range on a Nicolet Nexus FT-IR with CsI beamsplitter, using Nujol mulls between polyethylene sheets. C and H analyses were carried out with a PerkinElmer 240C microanalyzer. MALDI-TOF spectra were recorded in a Microflex MALDI-TOF Bruker spectrometer, and ESI mass spectra were recorded on an HP-5989B API-Electrospray mass spectrometer with a 59987A interface. Exact mass experiments were carried out in the same instrument as ESI mass experiments. ^1H, $^{13}C\{^1H\}$, ^{19}F, and $^{31}P\{^1H\}$ NMR spectra were recorded on a Bruker AVANCE 400 instrument in the appropriate solvent for each compound. Chemical shifts are quoted relative to $SiMe_4$ (external), $CFCl_3$ (external), and H_3PO_4 (85%) (external), respectively. The quantitative monitoring of reactions was performed by gas chromatography using a Hewlett-Packard G1800B GCD system, equipped with a Teknokroma TRB-1 cross-linked dimethylpolysiloxane column (30 m × 0.25 mm × 0.25 μm) and MS detector (electron impact with single quadrupole filter). A split injection system with a split ratio of 50:1 was used with helium as carrier gas at a head pressure of 16 psi. Temperature programming was 80 °C (2 min), 20 °C/min, 240 °C (10 min). The inlet temperature was 225 °C, and the detector temperature was 250 °C. Conversion of the starting material and product yield were measured by integrating the chromatographic peaks of phenylacetylene (retention time 2.45 min) and 2-methyl-2-phenyl-1,3-dioxolane (retention time 5.32 min). No internal or external standard was used since both compounds showed a similar response factor ($K_{2\text{-methyl-2-phenyl-1,3-dioxolane}}/K_{\text{phenylacetylene}}$ = 0.99).

Synthesis of $[AuClP(C_6H_4F)_3]$ (4). To a solution of $[AuCl(tht)]$ (0.780 mmol, 250.1 mg) in dichloromethane (25 mL) was added 0.780 mmol of tris(4-fluorophenyl)phosphine (246.7 mg). After 45 min of stirring, the solution was concentrated under vacuum. Finally, the addition of hexane (5 mL) led to the precipitation of product **4** as a white solid.

Yield: 89%. Anal. Calcd for **4** ($C_{18}H_{12}AuClF_3P$): C, 39.40; H, 2.20. Found: C, 39.05; H, 2.27. ^1H NMR (400 MHz, 298 K, $CDCl_3$): 7.51 (m, 6H, PC_6H_4F), 7.20 (m, 6H, PC_6H_4F). ^{19}F NMR (377 MHz, 298 K, $CDCl_3$): −105.4 (m). $^{31}P\{^1H\}$ NMR (162 MHz, 298 K, $CDCl_3$): 30.8 (s). $^{13}C\{^1H\}$ NMR (101 MHz, 298 K, $CDCl_3$): 165.3 (dd, C_{Ar}-F), 136.4 (dd, $C_{Ar}H$), 124.4 (dd, P-C_{Ar}), 117.1 (dd, $C_{Ar}H$). FT-IR (Nujol mull): 326 cm^{-1} ν(Au-Cl). MS (ESI+): calcd for $C_{18}H_{12}AuClF_3NaP$ $[M + Na]^+$ 570.9875; found 570.9886.

Preparation of $[P(Ph)_3Me]ClO_4$, $[P(C_6H_4OMe)_3Me]ClO_4$, and $[P(C_6H_4F)_3Me]ClO_4$. This synthesis is a modification of the

Scheme 4. Schematic Representation of the Different Catalyst Stabilities

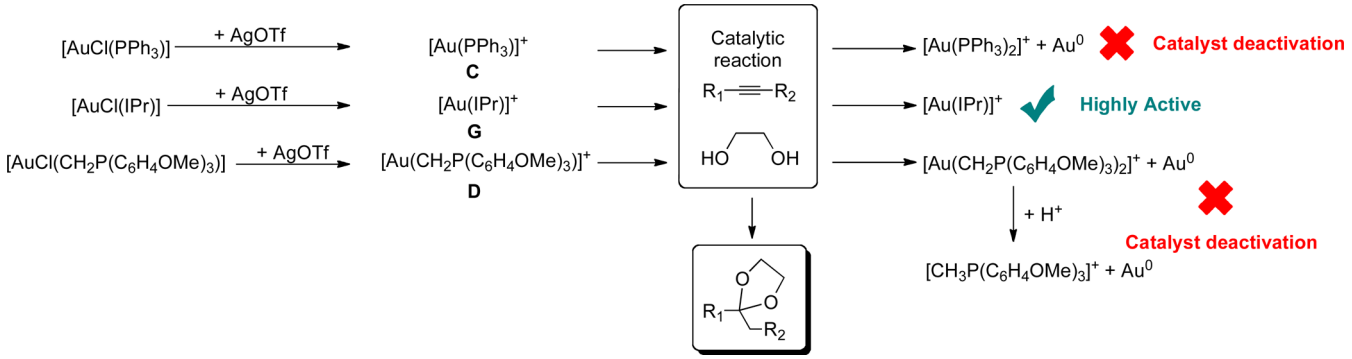

DOI: 10.1021/acs.organomet.5b01015
Organometallics XXXX, XXX, XXX−XXX

preparation of compound $[P(Ph)_3Me]ClO_4$.[32] Under an inert atmosphere, to a solution of the corresponding phosphine in toluene was added a stoichiometric amount of methyl iodide. After 6−8 h of stirring at refluxing temperature, a white precipitate appeared. Filtration of the solution allowed us to obtain the corresponding iodide salt. To a solution of this compound in dichloromethane was added a stoichiometric amount of silver perchlorate. After 7 h of stirring, the solution was filtered. Finally, concentration under vacuum and addition of hexane (5 mL) led to the precipitation of the corresponding products $[P(C_6H_4OMe)_3Me]ClO_4$ and $[P(C_6H_4F)_3Me]ClO_4$, as white solids.

$[P(C_6H_4OMe)_3Me]ClO_4$. Yield: 95%. Anal. Calcd for $[P(C_6H_4OMe)_3Me]ClO_4$ ($C_{22}H_{24}ClO_7P$): C, 56.60; H, 5.18. Found: C, 56.22; H, 5.16. ^{1}H NMR (400 MHz, 298 K, $CDCl_3$): 7.52 (m, 6H, $PC_6H_4OCH_3$), 7.14 (m, 6H, $PC_6H_4OCH_3$), 3.90 (s, 9H, OCH_3), 2.71 (d, 3H, CH_3). $^{31}P\{^1H\}$ NMR (162 MHz, 298 K, $CDCl_3$): 18.7 (s). FT-IR (Nujol mull): 1106, 624 cm^{-1} $\nu(ClO_4)$. MS (ESI+): calcd for $C_{22}H_{24}O_3P$ $[P(C_6H_4OMe)_3Me]^+$ 367.1458; found 367.1467. MS (ESI−): calcd for ClO_4 $[ClO_4]^-$ 98.9480; found 98.9486.

$[P(C_6H_4F)_3Me]ClO_4$. Yield: 92%. Anal. Calcd for $[P(C_6H_4F)_3Me]ClO_4$ ($C_{19}H_{15}ClF_3O_4P$): C, 52.98; H, 3.51. Found: C, 53.07; H, 3.49. ^{1}H NMR (400 MHz, 298 K, $CDCl_3$): 7.72 (m, 6H, PC_6H_4F), 7.39 (m, 6H, PC_6H_4F), 2.93 (d, 3H, CH_3). ^{19}F NMR (377 MHz, 298 K, $CDCl_3$): −99.1 (s). $^{31}P\{^1H\}$ NMR (162 MHz, 298 K, $CDCl_3$): 21.4 (s). FT-IR (Nujol mull): 1100, 623 cm^{-1} $\nu(ClO_4)$. MS (ESI+): calcd for $C_{19}H_{15}F_3P$ $[P(C_6H_4F)_3Me]^+$ 331.0858; found 331.0865. MS (ESI−): calcd for ClO_4 $[ClO_4]^-$ 98.9480; found 98.9482.

Synthesis of $[Au(C_6F_5)(CH_2P(C_6H_4F)_3)]$ and $[Au(C_6F_5)(CH_2P(C_6H_4OMe)_3)]$. This synthesis is a modification of the preparation of compound $[Au(C_6F_5)(CH_2PPh_3)]$.[25] In a Schlenk under an inert atmosphere was suspended 0.412 mmol of corresponding phosphonium salt ($[P(C_6H_4OMe)_3Me]ClO_4$ or $[P(C_6H_4F)_3Me]ClO_4$) in 25 mL of dry diethyl ether. Then 0.412 mmol of butyllithium and 0.412 mmol of $[Au(C_6F_5)(tht)]$ were added to the suspension to obtain a colorless solution, which was filtered. Finally, concentration under vacuum and addition of hexane (5 mL) led to the precipitation of the corresponding products, $[Au(C_6F_5)(CH_2P(C_6H_4F)_3)]$ and $[Au(C_6F_5)(CH_2P(C_6H_4OMe)_3)]$, as white solids.

$[Au(C_6F_5)(CH_2P(C_6H_4F)_3)]$. Yield: 43%. Anal. Calcd for $[Au(C_6F_5)(CH_2P(C_6H_4F)_3)]$ ($C_{25}H_{14}AuF_8P$): C, 43.25; H, 2.03. Found: C, 43.37; H, 1.92. ^{1}H NMR (400 MHz, 298 K, $CDCl_3$): 7.80 (m, 6H, PC_6H_4F), 7.27 (m, 6H, PC_6H_4F), 1.82 (d, 2H, CH_2). ^{19}F NMR (377 MHz, 298 K, $CDCl_3$): −103.0 (s, 3F, C_6H_4F), −116.9 (dd, 2F, F_{ortho}), −161.3 (t, 1F, F_{para}), −163.1 (m, 2F, F_{meta}). $^{31}P\{^1H\}$ NMR (162 MHz, 298 K, $CDCl_3$): 31.6 (s). FT-IR (Nujol mull): 1500, 953, 776 $\nu(C_6F_5)$, 526 cm^{-1} ν(Au−C). MS (ESI−): calcd for $C_{25}H_{13}AuF_8P$ $[M - H]^-$ 693.0298; found 693.0309.

$[Au(C_6F_5)(CH_2P(C_6H_4OMe)_3)]$. Yield: 52%. Anal. Calcd for $[Au(C_6F_5)(CH_2P(C_6H_4OMe)_3)]$ ($C_{28}H_{23}AuF_5O_3P$): C, 46.04; H, 3.17. Found: C, 45.92; H, 3.22. ^{1}H NMR (400 MHz, 298 K, $CDCl_3$): 7.65 (m, 6H, PC_6H_4OMe), 7.01 (m, 6H, PC_6H_4OMe), 3.86 (s, 9H, OCH_3), 1.77 (d, 2H, CH_2). ^{19}F NMR (377 MHz, 298 K, $CDCl_3$): −116.5 (dd, 2F, F_{orto}), −161.8 (t, 1F, F_{para}), −163.4 (m, 2F, F_{meta}). $^{31}P\{^1H\}$ NMR (162 MHz, 298 K, $CDCl_3$): 30.6 (s). FT-IR (Nujol mull): 1502, 951, 803 $\nu(C_6F_5)$, 528 cm^{-1} ν(Au−C). MS (ESI+): calcd for $C_{28}H_{23}AuF_5NaO_3P$ $[M + Na]^+$ 753.0863; found 753.0847.

Preparation of $[AuCl(CH_2PPh_3)]$ (5), $[AuCl(CH_2P(C_6H_4F)_3)]$ (6), and $[AuCl(CH_2P(C_6H_4OMe)_3)]$ (7). To a solution of $[Au(C_6F_5)(Y)]$ (0.250 mmol; Y = CH_2PPh_3, $CH_2P(C_6H_4F)_3$, $CH_2P(C_6H_4OMe)_3$) in diethyl ether at −10 °C was added an excess of a solution of HCl in diethyl ether. After 3−4 h of stirring a white precipitate appeared. Filtration of the solution allowed obtaining the corresponding product: **5**, **6**, or **7**.

*$[AuCl(CH_2PPh_3)]$ (**5**).* Yield: 61%. Anal. Calcd for **5** ($C_{19}H_{17}AuClP$): C, 44.86; H, 3.37. Found: C, 45.01; H, 3.42. ^{1}H NMR (400 MHz, 298 K, $CDCl_3$): 7.77−7.55 (m, 15H, C_6H_5), 2.12 (d, 2H, CH_2). $^{31}P\{^1H\}$ NMR (162 MHz, 298 K, $CDCl_3$): 30.3 (s). $^{13}C\{^1H\}$ NMR (101 MHz, 298 K, $CDCl_3$): 133.5 (d, $C_{Ar}H$), 133.2 (d, $C_{Ar}H$), 129.6 (d, $C_{Ar}H$), 125.7 (d, P-C_{Ar}), −1.2 (d, CH_2). FT-IR (Nujol mull): 512 ν(Au−C), 315 cm^{-1} ν(Au−Cl). MS (ESI+): calcd for $C_{19}H_{17}AuClNaP$ $[M + Na]^+$ 531.0314; found 531.0317.

*$[AuCl(CH_2P(C_6H_4F)_3)]$ (**6**).* Yield: 61%. Anal. Calcd for **6** ($C_{19}H_{14}AuClF_3P$): C, 40.55; H, 2.51. Found: C, 40.46; H, 2.60. ^{1}H NMR (400 MHz, 298 K, $CDCl_3$): 7.76 (m, 6H, PC_6H_4F), 7.27 (m, 6H, PC_6H_4F), 2.10 (d, 2H, CH_2). ^{19}F NMR (377 MHz, 298 K, $CDCl_3$): −102.3 (m). $^{31}P\{^1H\}$ NMR (162 MHz, 298 K, $CDCl_3$): 29.2 (s). $^{13}C\{^1H\}$ NMR (101 MHz, 298 K, $CDCl_3$): 166.0 (dd, C-F), 135.8 (dd, $C_{Ar}H$), 121.2 (dd, P-C_{Ar}), 117.6 (dd, $C_{Ar}H$), −0.1 (d, CH_2). FT-IR (Nujol mull): 522 ν(Au-C), 323 cm^{-1} ν(Au-Cl). MS (ESI+): calcd for $C_{19}H_{14}AuClF_3NaP$ $[M + Na]^+$ 585.0031; found 585.0013.

*$[AuCl(CH_2P(C_6H_4OMe)_3)]$ (**7**).* Yield: 64%. Anal. Calcd for **7** ($C_{22}H_{23}AuClO_3P$): C, 44.13; H, 3.87. Found: C, 44.25; H, 3.96. ^{1}H NMR (400 MHz, 298 K, $CDCl_3$): 7.63 (m, 6H, PC_6H_4OMe), 7.00 (m, 6H, PC_6H_4OMe), 3.86 (s, 9H, OCH_3), 2.02 (d, 2H, CH_2). $^{31}P\{^1H\}$ NMR (162 MHz, 298 K, $CDCl_3$): 27.8 (s). $^{13}C\{^1H\}$ NMR (101 MHz, 298 K, $CDCl_3$): 163.4 (d, C-OCH_3), 134.9 (d, $C_{Ar}H$), 117.0 (d, P-C_{Ar}), 115.1 (d, $C_{Ar}H$), 55.7 (s, OCH_3), 0.1 (d, CH_2). FT-IR (Nujol mull): 525 ν(Au-C), 309 cm^{-1} ν(Au-Cl). MS (ESI+): calcd for $C_{22}H_{23}AuClNaO_3P$ $[M + Na]^+$ 621.0631; found 621.0619.

General Procedure for the Catalytic Synthesis of Cyclic Acetals. *Catalysis at 100 °C during 4 h.* In a two-necked round-bottomed flask, evacuated and filled with nitrogen, were dissolved the alkyne (1 mmol), the ethylene glycol (1 mmol), the corresponding Au complex (0.02 mmol), and the silver salt, AgOTf (0.02 mmol), in 5 mL of toluene. The reaction was protected from light and placed at 100 °C with stirring. Aliquots of the reaction mixture (around 0.1 mL) were periodically withdrawn from the reactor and analyzed by GC-MS.

Catalysis at 75 °C during 1 h. We performed the test in a similar way but carrying out the reaction in ambient conditions at 75 °C.

Computational Details. All geometry optimizations were carried out using the M06-2X hybrid functional.[33] In all calculations, the heteroatoms were treated by SDD pseudopotentials,[34] including only the valence electrons for each atom. For these atoms double-ζ basis sets were used, augmented with d-type polarization functions.[35] For H atoms, a double-ζ basis set was used, together with a p-type polarization function.[36] The 19-valence electron SDD pseudopotential[37] was employed for Au atoms, together with two f-type polarization functions.[38] Full geometry optimizations and transition structure (TS) searches were carried out with the Gaussian 09 package.[39] The possibility of different conformations was taken into account for all structures. Frequency analyses were carried out at the same level used in the geometry optimizations, and the nature of the stationary points was determined in each case according to the appropriate number of negative eigenvalues of the Hessian matrix. Scaled frequencies were not considered. Mass-weighted intrinsic reaction coordinate (IRC) calculations were carried out by using the Gonzalez and Schlegel scheme[40,41] in order to ensure that the TSs indeed connected the appropriate reactants and products. Bulk solvent effects were considered implicitly by performing single-point energy calculations on the gas-phase optimized geometries, through the IEFPCM polarizable continuum model[42] as implemented in Gaussian 09. The internally stored parameters for toluene were used to calculate solvation free energies (ΔG_{solv}). Gibbs free energies (ΔG) were used for the discussion on the relative stabilities of the considered structures. The Au−L bond dissociation energies and the Au−π interaction energies were estimated using counterpoise correction for the BSSE.[43]

In the case of fragment $[AuPPh_3]^+$, all the attemps to fully optimize the model system using the DFT M06-2X functional failed. In order to overcome this problem, we performed a (QM/MM) ONIOM[44] optimization (DFT M06-2X functional/molecular mechanical (Universal Force Field, UFF)),[45] followed by a single-point full DFT calculation to obtain the energy of the fragment in the same conditions as other calculations. This methodology was proved with the fragment $[AuPMe_3]^+$, finding very similar results in terms of energy.

DOI: 10.1021/acs.organomet.5b01015
Organometallics XXXX, XXX, XXX−XXX

■ ASSOCIATED CONTENT

Supporting Information

The Supporting Information is available free of charge on the ACS Publications website at DOI: 10.1021/acs.organomet.5b01015.

Figures, tables, NMR spectra, and computational data (energies) (PDF)

Cartesian coordinates (XYZ)

■ AUTHOR INFORMATION

Corresponding Author

*E-mail: josemaria.lopez@unirioja.es.

Notes

The authors declare no competing financial interest.

■ ACKNOWLEDGMENTS

D.G.I. MINECO/FEDER (project number CTQ 2013-48635-C2-2-P) is acknowledged for financial support. J.C. also acknowledges MEC for an FPU grant. We gratefully thank CESGA for computer support.

■ REFERENCES

(1) Hashmi, A. S. K.; Toste, D. F.; Toste, F. D. *Modern Gold Catalyzed Synthesis*; Wiley, 2012.

(2) Corma, A.; Leyva-Pérez, A.; Sabater, M. J. *Chem. Rev.* **2011**, *111*, 1657−1712.

(3) Dorel, R.; Echavarren, A. M. *Chem. Rev.* **2015**, *115*, 9028−9072.

(4) Hashmi, A. S. K. *Chem. Rev.* **2007**, *107*, 3180−3211.

(5) Garcia, P.; Malacria, M.; Aubert, C.; Gandon, V.; Fensterbank, L. *ChemCatChem* **2010**, *2*, 493−497.

(6) Arcadi, A. *Chem. Rev.* **2008**, *108*, 3266−3325.

(7) Gorin, D. J.; Sherry, B. D.; Toste, F. D. *Chem. Rev.* **2008**, *108*, 3351−3378.

(8) Jiménez-Núñez, E.; Echavarren, A. M. *Chem. Rev.* **2008**, *108*, 3326−3350.

(9) Li, Z.; Brouwer, C.; He, C. *Chem. Rev.* **2008**, *108*, 3239−3265.

(10) Hashmi, A. S. K.; Rudolph, M. *Chem. Soc. Rev.* **2008**, *37*, 1766−1775.

(11) Rudolph, M.; Hashmi, A. S. K. *Chem. Soc. Rev.* **2012**, *41*, 2448−2462.

(12) Lauterbach, T.; Asiri, A. M.; Hashmi, A. S. K. In *Advances in Organometallic Chemistry*; Pérez, P. J., Ed.; Academic Press, 2014; Vol. *62*, pp 261−297.

(13) Nolan, S. P. *Acc. Chem. Res.* **2011**, *44*, 91−100.

(14) Pyykkö, P. *Angew. Chem., Int. Ed.* **2002**, *41*, 3573−3578.

(15) Pyykkö, P. *Angew. Chem., Int. Ed.* **2004**, *43*, 4412−4456.

(16) Schwarz, H. *Angew. Chem., Int. Ed.* **2003**, *42*, 4442−4454.

(17) Gorin, D. J.; Toste, F. D. *Nature* **2007**, *446*, 395−403.

(18) Leyva-Pérez, A.; Corma, A. *Angew. Chem., Int. Ed.* **2012**, *51*, 614−635.

(19) Wang, W.; Hammond, G. B.; Xu, B. *J. Am. Chem. Soc.* **2012**, *134*, 5697−5705.

(20) Santos, L. L.; Ruiz, V. R.; Sabater, M. J.; Corma, A. *Tetrahedron* **2008**, *64*, 7902−7909.

(21) Annibale, G.; Canovese, L.; Cattalini, L.; Natile, G. *J. Chem. Soc., Dalton Trans.* **1980**, 1017−1021.

(22) Angermaier, K.; Zeller, E.; Schmidbaur, H. *J. Organomet. Chem.* **1994**, *472*, 371−376.

(23) Ho, S. Y.; Tiekink, E. R. T. *Acta Crystallogr., Sect. E: Struct. Rep. Online* **2001**, *57*, m549−m550.

(24) de Frémont, P.; Scott, N. M.; Stevens, E. D.; Nolan, S. P. *Organometallics* **2005**, *24*, 2411−2418.

(25) Usón, R.; Laguna, A.; Laguna, M.; Usó, A.; Gimeno, M. C. *Synth. React. Inorg. Met.-Org. Chem.* **1988**, *18*, 69−82.

(26) Teles, J. H.; Brode, S.; Chabanas, M. *Angew. Chem., Int. Ed.* **1998**, *37*, 1415−1418.

(27) Ciancaleoni, G.; Belpassi, L.; Zuccaccia, D.; Tarantelli, F.; Belanzoni, P. *ACS Catal.* **2015**, *5*, 803−814.

(28) Fructos, M. R.; Urbano, J.; Díaz-Requejo, M. M.; Pérez, P. J. *Beilstein J. Org. Chem.* **2015**, *11*, 2254−2260.

(29) Although our catalyst model systems for DFT calculations were simplified to the naked cationic species $[AuL]^+$ for the sake of lowering the computational cost, it is also very likely that [AuL(TfO)] or [AuL(S)]TfO (S = solvent molecule) could also be involved in the mechanism.

(30) Zhdanko, A.; Ströbele, M.; Maier, M. E. *Chem. - Eur. J.* **2012**, *18*, 14732−14744.

(31) de Frémont, P.; Marion, N.; Nolan, S. P. *J. Organomet. Chem.* **2009**, *694*, 551−560.

(32) Smith, M. B.; March, J. *March's Advanced Organic Chemistry: Reactions, Mechanisms, and Structure*; Wiley, 2007.

(33) Zhao, Y.; Truhlar, D. *Theor. Chem. Acc.* **2008**, *120*, 215−241.

(34) Bergner, A.; Dolg, M.; Küchle, W.; Stoll, H.; Preuß, H. *Mol. Phys.* **1993**, *80*, 1431−1441.

(35) Huzinaga, S.; Andzelm, J. *Gaussian Basis Sets for Molecular Calculations*; Elsevier, 1984.

(36) Huzinaga, S. *J. Chem. Phys.* **1965**, *42*, 1293−1302.

(37) Andrae, D.; Häußermann, U.; Dolg, M.; Stoll, H.; Preuß, H. *Theor. Chim. Acta* **1990**, *77*, 123−141.

(38) Pyykkö, P.; Runeberg, N.; Mendizabal, F. *Chem. - Eur. J.* **1997**, *3*, 1451−1457.

(39) Frisch, M. J.; Trucks, G. W.; Schlegel, H. B.; Scuseria, G. E.; Robb, M. A.; Cheeseman, J. R.; Scalmani, G.; Barone, V.; Mennucci, B.; Petersson, G. A.; Nakatsuji, H.; Caricato, M.; Li, X.; Hratchian, H. P.; Izmaylov, A. F.; Bloino, J.; Zheng, G.; Sonnenberg, J. L.; Hada, M.; Ehara, M.; Toyota, K.; Fukuda, R.; Hasegawa, J.; Ishida, M.; Nakajima, T.; Honda, Y.; Kitao, O.; Nakai, H.; Vreven, T.; Montgomery, J.; Peralta, J. E.; Ogliaro, F.; Bearpark, M.; Heyd, J. J.; Brothers, E.; Kudin, K. N.; Staroverov, V. N.; Kobayashi, R.; Normand, J.; Raghavachari, K.; Rendell, A.; Burant, J. C.; Iyengar, S. S.; Tomasi, J.; Cossi, M.; Rega, N.; Millam, J. M.; Klene, M.; Knox, J. E.; Cross, J. B.; Bakken, V.; Adamo, C.; Jaramillo, J.; Gomperts, R.; Stratmann, R. E.; Yazyev, O.; Austin, A. J.; Cammi, R.; Pomelli, C.; Ochterski, J. W.; Martin, R. L.; Morokuma, K.; Zakrzewski, V. G.; Voth, G. A.; Salvador, P.; Dannenberg, J. J.; Dapprich, S.; Daniels, A. D.; Farkas, Ö.; Foresman, J. B.; Ortiz, J. V.; Cioslowski, J.; Fox, D. J. *Gaussian 09*, Revision A02; Gaussian Inc: Wallingford, CT, 2009.

(40) Gonzalez, C.; Schlegel, H. B. *J. Chem. Phys.* **1989**, *90*, 2154−2161.

(41) Gonzalez, C.; Schlegel, H. B. *J. Phys. Chem.* **1990**, *94*, 5523−5527.

(42) Scalmani, G.; Frisch, M. J. *J. Chem. Phys.* **2010**, *132*, 132.

(43) Boys, S. F.; Bernardi, F. *Mol. Phys.* **1970**, *19*, 553−566.

(44) Vreven, T.; Morokuma, K. *J. Comput. Chem.* **2000**, *21*, 1419−1432.

(45) Rappe, A. K.; Casewit, C. J.; Colwell, K. S.; Goddard, W. A.; Skiff, W. M. *J. Am. Chem. Soc.* **1992**, *114*, 10024−10035.

DOI: 10.1021/acs.organomet.5b01015
Organometallics XXXX, XXX, XXX−XXX